energies

MDPI

Article

An ECMS for Multi-Objective Energy Management Strategy of Parallel Diesel Electric Hybrid Ship Based on Ant Colony Optimization Algorithm

Yongbing Xiang [1,*] and Xiaomin Yang [2]

[1] School of Energy and Power Engineering, Wuhan University of Technology, Wuhan 430063, China
[2] School of Mechatronics Engineering, Henan University of Science and Technology, Luoyang 471003, China; sdqc2012gfs@163.com
* Correspondence: xybxiang@163.com or xybxiang@whut.edu.cn

Abstract: In order to reduce fuel consumption and reduce the deviation between the final battery state-of-charge (SOC) value and the target value at the same time, a novel double-layer multi-objective optimization method is proposed, which adopts an improved ant colony optimization (ACO) algorithm and the equivalent fuel consumption minimization strategy (ECMS) considering mode switching. The proposed strategy adopts a two-layer structure. In the inner layer, the ECMS considering mode switching was adopted to optimize the working mode and working point, so as to achieve the goal of reducing fuel consumption. In the outer layer, aiming at the shortcomings of traditional ACO, the heuristic factor and adaptive volatilization factor were introduced. An improved ACO method was proposed to optimize the equivalent factor, so as to achieve the goal of reducing the deviation between the final value of SOC and the target value. In order to verify the effectiveness of the proposed algorithm, it is compared with the traditional ECMS strategy and the rule-based (RB) ECMS strategy. The simulation results show that the proposed energy management strategy combining an improved ACO algorithm with ECMS considering mode switching can reduce the energy consumption of the whole ship and control the battery power.

Keywords: diesel electric hybrid; ECMS; ACO; multi-objective optimization; energy management

Citation: Xiang, Y.; Yang, X. An ECMS for Multi-Objective Energy Management Strategy of Parallel Diesel Electric Hybrid Ship Based on Ant Colony Optimization Algorithm. *Energies* **2021**, *14*, 810. https://doi.org/10.3390/en14040810

Academic Editor: Spyros Voutetakis
Received: 9 January 2021
Accepted: 2 February 2021
Published: 4 February 2021

1. Introduction

The energy crisis has become a global problem. In order to solve the increasingly poor natural energy and environmental health, and realize the sustainable development of the shipbuilding industry, it is an inevitable choice for the development of human society to establish a clean and renewable new energy system. Hybrid ships have the advantages of low emission, low noise, high thermal efficiency, remarkable environmental protection effect, and the improved energy structures, which has become the inevitable development trend of the shipbuilding industry [1]. A hybrid ship is a ship equipped with two or more power sources. At present, the structure and operating conditions of the ship power system are becoming more and more complex and diversified, so it is of great significance to study the optimal control strategy of energy under various operating conditions [2]. How to allocate the energy of each power source, optimize the energy management of the whole ship power system in real time, and reduce the fuel energy consumption of the whole ship as much as possible is one of the key technologies to promote the rapid development of hybrid ships [3]. The energy management control system is a difficult point in the research of hybrid ships due to nonlinear, multivariable, time-varying, and other factors [4]. The advantages and disadvantages of its control strategy directly affect the power performance, economy, and emissions of hybrid ships. The main objective of energy management strategy optimization of hybrid ships is to reduce the fuel consumption of the whole ship [5]. In some cases, it is desirable to control the battery power near a

certain target value. In order to further avoid the error caused by the conversion of fuel consumption into power consumption, it is generally hoped to control the error within 1% [6]. Therefore, reducing the energy consumption of the whole ship and controlling the battery power become the two goals of energy management of diesel electric hybrid ships.

A large number of studies in the literature put forward different energy management strategies from different perspectives [7]. This paper clearly introduces the development of ship energy system optimization [8]. Among them, the rule-based management strategy is mainly based on engineering experience or experimental data to repeatedly debug the control threshold, so it is easy to achieve, has good robustness, and has low development cost, but it depends on the level of experience and has poor adaptability to working conditions [9]. Gao et al. [10] proposed a method for forecasting ship load demand based on the real-time classification of different working conditions to effectively optimize the load distribution among the power sources during the navigation of a hybrid ship. The simulation results showed that the proposed model has high accuracy under different conditions, and it was an effective means to predict the load demand of hybrid electric ships. The energy management strategy based on global optimization needs to predict the driving condition information, so it has certain limitations and is difficult to be used in real ship control [11]. The equivalent fuel consumption minimization strategy (ECMS) has the advantages of simple structure, small amount of computation, and no prior knowledge. By introducing a penalty function, the strategy has good power retention characteristics, which makes it more suitable for energy management in the power retention stage of plug-in hybrid electric vehicles [12]. Tian et al. [13] proposed an adaptive energy management system composed of offline and online parts to improve the energy efficiency of parallel hybrid electric buses. Therefore, it has been widely studied. However, the ECMS strategy is rarely used in hybrid ships [14]. Haseltalab et al. [15] proposed a control method for hybrid power ship energy management, which took into account the uncertainty in the ship model and the interference of the surrounding environment. The nonlinear robust tube-based model predictive control (NRTB-MPC) was used to control the speed and calculate the energy required for ship propulsion. Dedes et al. [16] proposed the application of a diesel hybrid system in slow ocean-going ships. The results showed that the fuel of the auxiliary load was saved because there was no conversion loss.

The ECMS strategy was first proposed by Paganelli [17]. The core idea used an equivalent factor to convert the electric energy consumption into fuel consumption, so that the global optimization problem transformed into an instantaneous optimization problem [18]. Compared with the global optimization algorithm, its computational complexity is lower. It does not need the information of future working conditions [19]. It can obtain the approximate optimal control effect. In theory, it can be applied to the actual ship control, which is considered to be the most promising application to real ships [20–22]. The equivalent factor is an important parameter in the ECMS algorithm that affects the torque distribution of the control strategy, which is the key to the optimization effect of ECMS [17]. Different values determine the different energy distribution between engine and battery, resulting in different ship energy consumption and battery power consumption. Therefore, the advanced intelligent algorithm is used to optimize the equivalent factor in real time, so as to achieve the control goal of battery power.

There are many methods to solve multi-objective optimization problems. Among them, the ant colony optimization (ACO) algorithm is simple, easy to implement, has efficient search ability, and has good versatility, which is suitable for dealing with various types of objective functions and constraint. Yang et al. [23] proposed a partial swarm optimization algorithm that was used to solve a multi-objective problem. This paper took a solar–diesel hybrid ship with 5000 car spaces as the research object. A multi-objective optimization model related to diesel generator's efficiency and the ship's fuel economy and was established. The results showed that the proposed energy management strategy took into account both diesel generator efficiency and ship economy, which could reduce ship fuel consumption and improve the service life of the diesel generator. Wei [24] proposed a

task scheduling optimization strategy using an improved ACO algorithm in cloud computing in order to solve the problems of load imbalance, slow convergence, and low resource utilization of a virtual machine in the existing task scheduling optimization strategy. Firstly, a scheduling model using an improved ant colony algorithm was proposed to avoid the dilemma of local optimization. Then, combined with the three objectives of the shortest waiting time, resource load balancing degree, and task completion cost, the task scheduling satisfaction function was constructed to find the optimal solution of task scheduling. Finally, the reward and penalty coefficient was introduced to optimize the pheromone updating rules of the ant colony algorithm to speed up the solution. Stodola [25] proposed a hybrid ant colony optimization algorithm. The algorithm combined probability technology and precision technology. The former was based on the behavior of ants in nature and simulated the annealing principle. The latter was a supplement to the former. The experimental results showed that this proposed algorithm overcomes the shortcomings of other methods because it has the smallest average error (the difference between the found solution and the known solution) over the entire set of benchmark examples. Ning et al. [26] created a new pheromone that was temporarily called a negative pheromone and proposed a new multi-objective ant colony optimization algorithm based on decomposition (NMOACO/D), which combined a multi-objective evolutionary algorithm based on decomposition ant colony optimization (MOEA/D-ACO) with negative pheromone. The results showed that the correct use of information related to the dominance solution could further improve the performance of the ACO algorithm. Zhao et al. [27] proposed an improved ACO algorithm for omnidirectional mobile vehicle path planning. The purpose of the improved ant colony algorithm is to design an appropriate route to connect the start and end of the environment with the obstacles.

In addition, the pheromone evaporation coefficient is segmented and adjusted to effectively balance the convergence speed and search ability. The numerical simulation showed the validity of the theoretical results. Zhao et al. [28] proposed a multi-objective optimization model based on cost, carbon emissions, and customer satisfaction in order to improve the performance and current situation of the cost minimization model widely used in the cold chain logistics and distribution process. The simulation results showed that the proposed system successfully provides a reference for the path optimization of cold chain logistics companies. Wang et al. [29] improved ACO to schedule time-triggered flows in time-sensitive networks (TSN). The simulation results showed that the improved ACO algorithm can schedule the time-triggered traffic in TSN well, and it was superior to the traditional ACO algorithm in convergence speed, optimization ability, and the ease of local optimal traps. The results showed that the proposed method provided an effective real-time guarantee for the TSNs. Jiao et al. [30] proposed an intelligent wheelchair path planning method based on adaptive polymorphic ACO. In order to avoid the ant colony falling into local optimum in the process of solving, adaptive state transition strategy and adaptive information update strategy were adopted in the polymorphic ant colony algorithm to ensure the relative importance of pheromone strength and desirability. The adaptive polymorphic ACO was used for target path planning and obstacle path planning, respectively. The results showed that compared with the improved ant colony algorithm and polymorphic ant colony algorithm, this method had better performance.

This paper used a 200 t parallel diesel electric hybrid boat as the research object, which has significant advantages in energy saving, but a variety of working modes also bring challenges to the energy management strategy. The energy management strategy of a parallel hybrid electric ship needs to optimize the working modes and working point at the same time. Therefore, this paper proposes the energy management strategy of ECMS, considering mode switching, and it completes the optimization of the above two aspects at the same time. In addition, the equivalent factor is an important parameter of ECMS. Different values determine the energy distribution of engine and battery, which leads to different energy consumption of the whole ship and battery. Therefore, the control target of battery power can be further realized by optimizing the equivalent factor. In order to solve

the above problems, this paper aims to reduce fuel consumption and reduce the deviation between the final SOC value and the target value.

In order to reduce ship energy consumption and control battery SOC at the same time, a multi-objective bi-level optimization energy management strategy based on the improved ACO is proposed for a parallel diesel electric hybrid ship. The proposed strategy adopts a two-layer structure. The inner layer used the ECMS considering mode switching to optimize the operating point, so as to achieve the goal of energy saving. The outer layer used improved ACO to optimize the equivalent factor iteratively to achieve the control of battery power.

The main contributions of this paper are as follows:

1. In order to achieve the goal of reducing fuel consumption, the equivalent fuel consumption minimization strategy considering mode switching was adopted to optimize the working mode and working point. It was no longer dependent on engineering experience and a calibration test to select the working mode.
2. In order to reduce the deviation between the final value of state of charge (SOC) and the target value, aiming at the shortcomings of traditional ACO, it is easy to fall into local optimum in the early stage and slowly down in the late stage. The premature convergence is easy to fall into local optimum and unable to converge globally. The heuristic factor and adaptive volatilization factor were introduced to improve these shortcomings. An improved ACO method was proposed to optimize the equivalent factor.
3. In order to verify the effectiveness of the proposed algorithm, it was compared with a traditional ECMS strategy and rule-based (RB)-ECMS strategy. The simulation results showed that the proposed energy management strategy combining an improved ACO algorithm with ECMS considering mode switching could optimize the working points of the engine and motor, reduce the energy consumption of the whole ship, maintain the deviation between the final value of SOC and the target value within a reasonable range, and control the battery power.

The rest of the paper is arranged as follows: Section 2 introduces the parallel hybrid diesel electric hybrid ship model and model validation. Section 3 introduces the proposed ECMS considering mode switching for energy optimization. Section 4 introduces the improved ACO control strategy. Section 5 presents the results of the analysis. Section 6 summarizes the main conclusions of the paper.

2. Establishment and Verification of Simulation Model

A parallel diesel electric hybrid 200 t tuna longline fishing boat is taken as the research object. The structure of a parallel diesel electric hybrid system is shown in Figure 1. The engine and motor can drive the propeller separately or mix; it can drive the propeller and charge battery. The working modes are divided into the hybrid drive mode, the diesel engine drive mode, the motor drive mode, and the diesel engine drive generator mode. The main parameters of the ship are shown in Table 1.

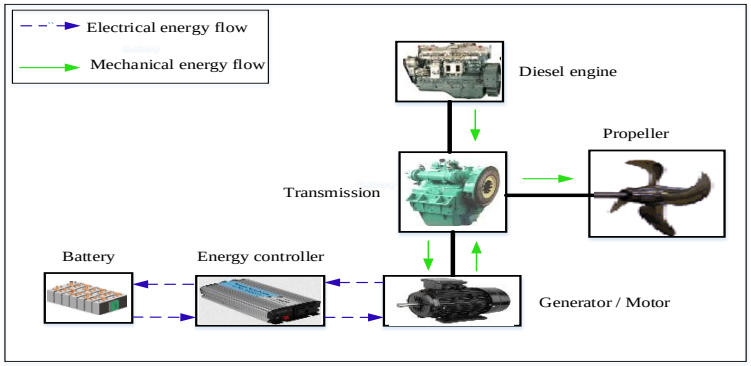

Figure 1. Structure diagram of power system of the tuna longline fishing boat.

Table 1. Main parameters.

Component	Parameter	Value
Engine	Type	Diesel engine
	Maximum torque [Nm]	2500
	Maximum speed [r/min]	1700
Motor	Type	Triple-phase asynchronous motor
	Maximum torque [Nm]	1348
	Maxim um speed [r/min]	5948
	Rated voltage [V]	380
Battery	Type	Ni-Mh battery
	Nominal capacity [Ah]	80
	Nominal voltage [V]	1.2
Transmission	Maximum main transmission ratio	6.27
	PTI transmission ratio	5.94
Propeller	Number of leaves	4
	Maximum speed [r/min]	303

2.1. Engine Model

The energy optimization of a parallel hybrid electric ship needs the fuel consumption of an engine. Considering the complexity of the engine, a quasi-static model was established. The fuel rate m can be expressed as [12,31]:

$$\dot{m_f} = f_{fuel}(T_e, \omega_e) \tag{1}$$

where ω_e and T_e are the engine speed and torque, respectively.

$$P_{\mathrm{e}} = H_{\mathrm{LHV}}\dot{m}_{\mathrm{f}} \tag{2}$$

where P_{e} represents the available power of the engine, and H_{LHV} represents the lower calorific value of fuel.

Figure 2a shows the brake-specific fuel consumption (BSFC) map of the diesel engine, whose black line represents the maximum torque under different speeds. Figure 2b shows the Manifold Absolute Pressure (MAP) of working efficiency of a diesel engine.

2.2. Motor Model

The motor is a three-phase asynchronous motor that can be used as a traction motor to provide torque and also as generator to charge the battery. Therefore, the motor power P_{m} can be expressed as [13]:

$$P_{\mathrm{m}} = \begin{cases} \frac{T_{\mathrm{m}} \cdot \omega_{\mathrm{m}}}{9550\eta_{\mathrm{em}}}, T_{\mathrm{m}} > 0 \\ \frac{T_{\mathrm{m}} \cdot \omega_{\mathrm{m}} \cdot \eta_{\mathrm{ge}}}{9550}, T_{\mathrm{m}} < 0 \end{cases} \tag{3}$$

where ω_{m} is the motor speed; η_{em} is the motor driving motor efficiency; and η_{ge} is the efficiency of the motor as a generator. η_{em} and η_{ge} can be obtained by querying Figure 2c. The motor efficiency map is presented in Figure 2c.

2.3. Battery Model

Ignoring the influence of temperature on the battery, the ring model was used to model the battery, and the expressions of SOC and output power were obtained as follows [13]:

$$\dot{SOC} = -\frac{U_{oc} - \sqrt{U_{oc}^2 - 4P_{\mathrm{bat}}R_{\mathrm{b}}}}{2Q_{\mathrm{b}}R_{\mathrm{b}}} \tag{4}$$

$$P_{\mathrm{bat}} = -\dot{SOC} \cdot U_{\mathrm{oc}} \cdot Q_{\mathrm{b}} \tag{5}$$

where SOC is the battery SOC change rate; U_{oc} is the battery open circuit voltage; R_b is the internal resistance of the battery; Q_b is the maximum capacity of the battery; and P_{bat} is the output power of the battery. Figure 2d is the battery equivalent circuit diagram.

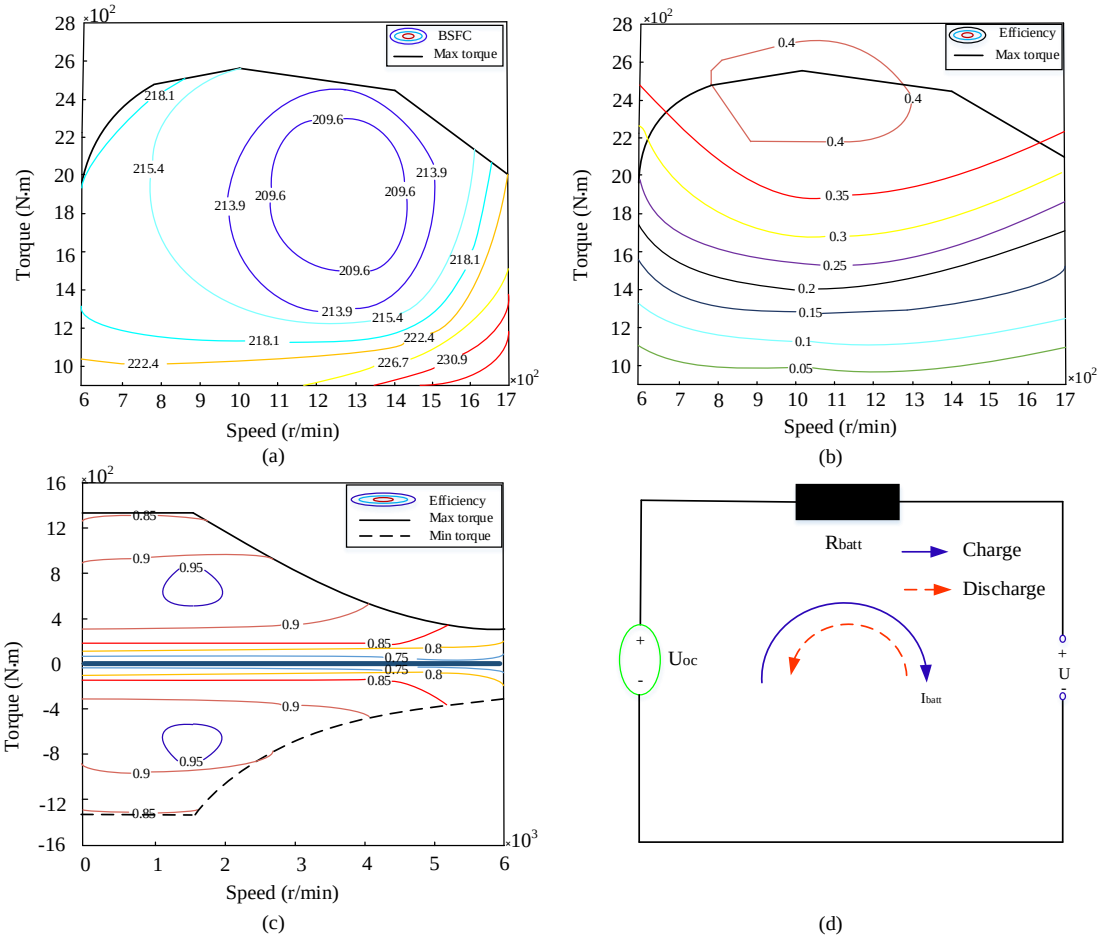

Figure 2. (**a**) MAP of the engine. (**b**) Efficiency MAP of the engine. (**c**) Efficiency MAP of the motor. (**d**) Battery equivalent circuit diagram.

2.4. Transmission System Model

In this paper, a double reduction ratio is used to transfer power, which consists of the main reduction ratio and Power Take In (PTI) reduction ratio [8].

$$\begin{cases} T_2 = i \times T_1 \\ n_1 = i \times n_2 \end{cases} \tag{6}$$

where T_2 and n_2 are the torque and speed of the output; T_1 and n_1 are the torque and speed of the input. i is the transmission ratio of the transmission system.

The torque synthesis device adopts a parallel gear box. At this time, only the superposition of torque is considered. The modeling is as follows:

$$T_{out} = T_{in1} + T_{in2} \tag{7}$$

where T_{in1} and T_{in2} are input torque; T_{out} is the output torque.

2.5. Four Quadrant Propeller Model

Using the dimensional analysis method, they are expressed by dimensionless quantity as follows [6]:

$$\mathrm{T} = K_T \rho n^2 D_P^4 \tag{8}$$

$$Q = K_Q \rho n^2 D_p^5 \tag{9}$$

$$\mathrm{J} = \frac{h_p}{D_P} = \frac{v_p}{nD_p} \tag{10}$$

where T is the propeller thrust, N; Q is the propeller torque, Nm; J is the propeller speed ratio, D_p is the propeller diameter, m; n is the propeller speed, ρ is the density of seawater, K_Q, K_T are the propeller torque coefficient and thrust coefficient respectively, and v_p is the speed of the propeller, m/s.

2.6. Propulsion System Model

The kinematic equations of the ship and propeller are written as [16]:

$$\mathrm{m}\frac{dv_s}{dt} = T - R_t \tag{11}$$

$$\pi\frac{dn}{dt} M_d i - M_p - M_\mathrm{f} \tag{12}$$

where v_s is the speed of the ship, m/s; R_t is the resistance of the ship, N; M_p is the torque output by the diesel engine, Nm; M_p is the resistance moment, Nm; and i is the reduction ratio of the gearbox.

$$R_t = f(v_s) \tag{13}$$

where $R_t = \lambda v_\theta^s$, where λ is the ship resistance coefficient and θ is a constant.

2.7. Model Validation

The diesel electric hybrid power system model of the tuna longline fishing boat was modeled by Matlab/Simulink software. The actual fishing conditions of the tuna longline fishing boat are very complex. The conditions of a complete cycle (T) include the full speed navigation conditions (T1), the rope-throwing conditions (T2), and the rope-lifting conditions (T3). The detailed working conditions of the tuna longline fishing boat are as follows. For the full speed operation condition, the demand speed is 12 kn, the working hours is 4 h, and the power source demand power is 335 kW. For the rope operation condition, the demand speed is 6 kn, the working hours is 6 h, and the power source demand power is 134 kW. For the hoisting condition, the demand speed is 3 kn, the working hours is 14 h, and the power source demand power is 50 kW.

The single fishing cycle of a tuna longline fishing boat is 24 h as the simulation time. The speed simulation diagram and the power distribution between the diesel engine and electric motor of a hybrid fishing boat in one fishing cycle are shown in Figure 3. From the speed simulation diagram, the motor power output diagram, and diesel engine output diagram, it can be seen that the simulation values are in good agreement with the experimental value, which verifies the correctness of the model.

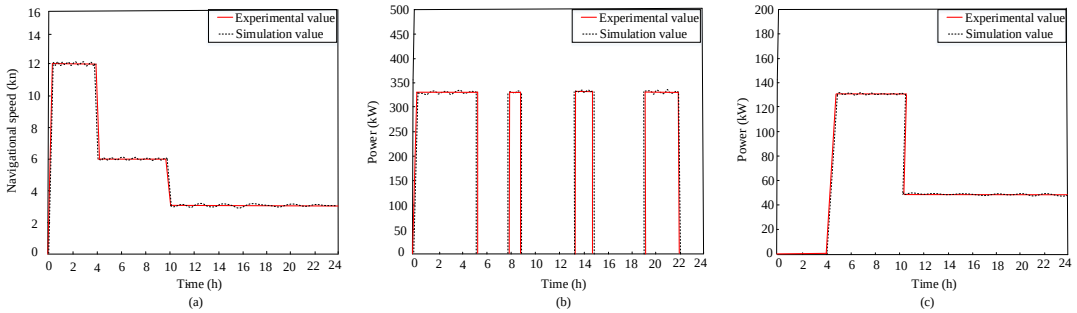

Figure 3. (**a**) Speed comparison. (**b**) Motor output power. (**c**) Output power of diesel engine.

3. ECMS Considering Mode Switching for Energy Optimization

ECMS Expression

According to the principle of ECMS control strategy [13], the whole instantaneous equivalent fuel consumption can be expressed as follows:

$$P_{eqv,hev} = P_{ef} + s \times P_s \tag{14}$$

$$P_{ef} = m \times Q_{LHV} \tag{15}$$

where, $P_{eqv,hev}$ is the total equivalent fuel consumption; P_{ef} is the power corresponding to the fuel consumed by the engine, s is the equivalent factor, P_s is the power consumed by the battery, $\dot{m}^*$ is the fuel consumption of the engine, and QLHV is the low calorific value of diesel.

Since the research object of this paper is a parallel diesel electric hybrid fishing ship, the input speed of the transmission is given when the off-line simulation is carried out. The required torque and equivalent factor s are used to obtain the torque distribution results under different demands [17]. The output torque of the motor and engine meets the requirements of navigation [12].

$$T_{req} = T_m + T_e \tag{16}$$

where T_{req} is the demand torque; T_m is the motor torque; and T_e is the engine torque.

The system satisfies the following constraints:

$$\begin{cases} 0 \le T_e \le T_{e,max} \\ T_{m,min} \le T_m \le T_{m,max} \\ P_{s,min} \le P_s \le P_{s,max} \\ T_{req} \le T_{m,max} + T_{e,max} \\ \omega_{e,dle} \le \omega_e \le \omega_{e,max} \\ \omega_{m,min} \le \omega_m \le \omega_{m,max} \\ S_{bat,min} \le S_{bat} \le S_{bat,max} \end{cases} \tag{17}$$

where $\omega_{e,dle}$ is the engine idling speed; $\omega_{e,max}$ is the engine maximum speed; $\omega_{m,min}$ is the motor minimum speed; $\omega_{m,max}$ is the motor maximum speed; $S_{bat,min}$ is the SOC minimum value; and $S_{bat,max}$ is SOC maximum value.

When the torque of the diesel engine is selected as the control variable, the optimal solution of the diesel engine and motor can be expressed as follows:

$$\begin{cases} T_e^* = \text{argmin}\left(m_{eqv,hev}\right) \\ T_m^* = T_{req} - T_e^* \end{cases}. \tag{18}$$

Considering that the equivalent factor in ECMS itself is the efficiency of oil to electricity conversion, it includes not only the charging and discharging efficiency of the battery, but also the efficiency of the motor, diesel engine, and transmission system. In order to simplify the research, this paper assumes that the SOC of the battery is a constant value in the offline simulation.

The required power of ship navigation is equal to the sum of motor output power and diesel engine output power [12]:

$$P_{\text{req}} = P_e + P_m. \tag{19}$$

The equivalent fuel consumption power of hybrid drive can be expressed as:

$$P_{eqv,hw} = a_e P_e + b_e + s(a_m P_m + b_m)\ . \tag{20}$$

By introducing Equation (19) into Equation (20), we can get:

$$\begin{aligned} P_{eqy,hw} &= a_e P_e + b_e + s\left(a_m\left(P_{req} - P_e\right) + b_m\right) \\ &= (a_e - s a_m)P_e + s a_m P_m + s b_m + b_e \end{aligned}. \tag{21}$$

At present, the energy management strategy of parallel diesel electric hybrid ships adopts the rule-based method to determine the working mode and then determines the optimal working point according to the ECMS [13]. This strategy separates the work mode from the work point optimization, and it constantly modifies and verifies the mode-switching rules through the real ship debugging, which results in heavy workload and can not guarantee the best economy. In order to solve the above problems, an ECMS energy management strategy considering mode switching is proposed. In this strategy, mode selection and work point optimization are considered together, and the optimization algorithm is used to replace the engineering experience and real ship debugging so as to ensure the optimization effect. In Figure 4, n_{mode} represents the number of optional working modes, and the input is the data of sailing conditions, including speed and the required torque of the whole ship. Then, according to the ECMS strategy, the equivalent fuel consumption of each working point of a certain mode is calculated, and the working point with the lowest equivalent fuel consumption is selected as the optimal working point of the mode [18]. The optimal working points of all the optional working modes are calculated, and the one with the lowest equivalent fuel consumption is selected as the optimal working point of the working mode, and the corresponding working mode is the optimal working mode of the working mode. The switching relationship between the driving modes is shown in Figure 5. The ECMS flow chart considering mode switching is shown in Figure 4.

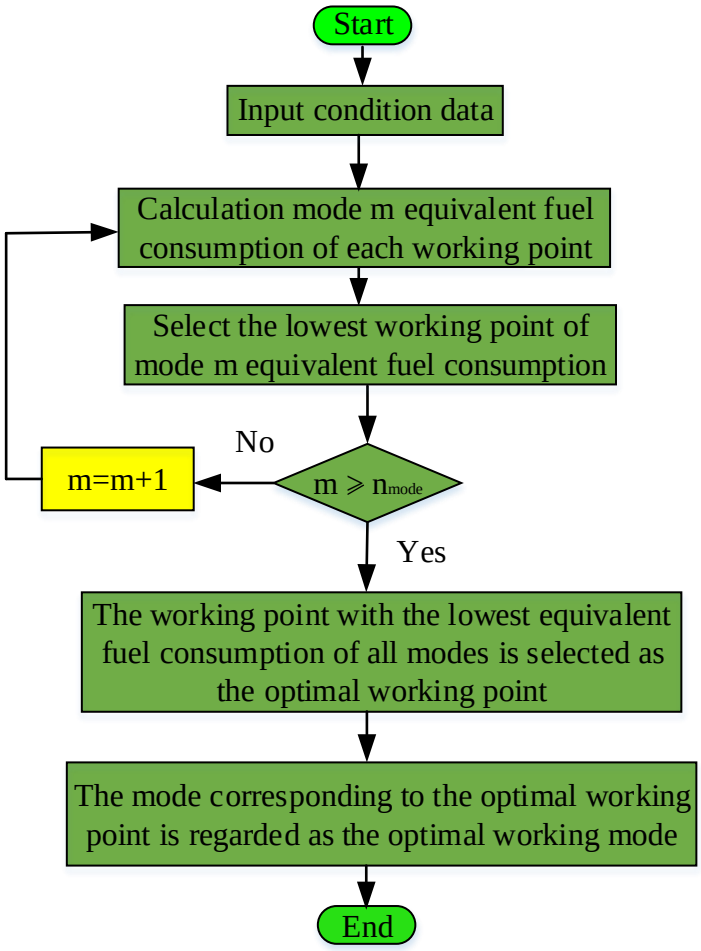

Figure 4. The equivalent fuel consumption minimization strategy (ECMS) flow chart considering mode switching.

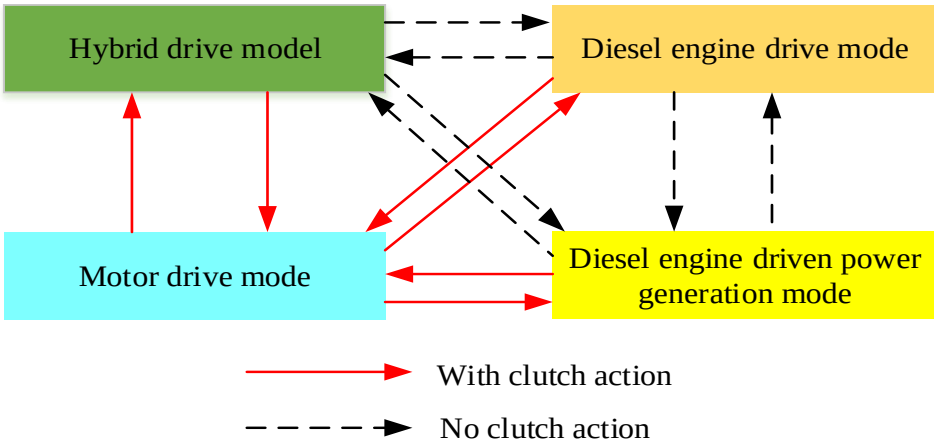

Figure 5. The working mode switching state diagram.

4. The ACO Algorithm

4.1. Basic Process of Ant Colony Algorithm

1. Initialization process of ant colony algorithm

M ants of a given number are randomly distributed in the equipartitioned random positions in the domain [*a*,*b*] of the solution [26]. The random distribution formula of the initial position of each ant (22) is generated as follows:

$$x(i,k) = a(k) + \frac{b(k) - a(k)}{M}(i - 1 + \text{rand}(0,1)). \tag{22}$$

The pheromone size of the initial position is as follows:

$$\Delta\tau_{x(i)} = e^{-F(x_i)}. \tag{23}$$

$F_{max}(x)$, $F_{min}(x)$ are the maximum and minimum objective function values, respectively. Generally, the physical meaning is path length or energy size.

2. The moving process of ant colony

Global search: The initialization process is the first search process of all ants. After the initialization, the position of each ant represents a solution, but only the position of one ant is the optimal solution of the first search. Other ants that do not find the optimal solution will conduct a global search, and the path of global search will move according to the pheromone of the ant with the optimal solution [27]. The rule of transition probability is shown in Equation (24).

$$P_{i,best} = \frac{e^{\tau_{X(b\in1)} - \tau_{X(i)}}}{e^{\tau_{X(\text{bett})}}} \tag{24}$$

In the process of global search, that is, when the ant moves to the optimal solution, it is possible to find a better solution than the optimal solution on the way of moving. Let the *n*-th ant of global search move to the optimal position, and the step size is as follows:

$$X_i = \begin{cases} X_i + \lambda(X_{best} - X_i), P_{i,best} > P_{set} \\ X_l + \text{rand}(-1,1) \cdot \frac{b-a}{M}, otherwise \end{cases}. \tag{25}$$

Among these, $0 < \lambda < 1$, $0 < P_{set} < 1$.

In the process of global search of other ants, the ants that get the optimal solution will carry out local search, and they will move in the radius around their position [27]. If they find a better solution in the process of moving, they will replace it. The original optimal

solution becomes the new optimal solution. The search calculation method is shown in Equation (26).

$$X_{Best} = \begin{cases} X_{is}, F(X_{is}) < F(X_{Best}) \\ X_{Best}, \ otherwise \end{cases} \tag{26}$$

3. Pheromone update rules

In each iteration, after all ants complete the global search and local search, the amount of information at each ant is updated. The update rules are shown in Equation (27).

$$\tau_{X(i)} = (1-\rho)\tau_{X(i)} + \Delta\tau_{X(i)} \tag{27}$$

The optimization process of the ant colony algorithm can be summarized as follows:

step 1: Set the maximum number of iterations, n_{max}, the number of ants in ant colony, M, and the value of solution, especially the value of solution.

step 2: Initialize according to Equations (22) and (23), including the position of all ants and the corresponding pheromone size.

step 3: The optimal solution position of the ant in each iteration is determined by the size of the pheromone.

step 4: In each iterative search process, each ant performs global search and local search according to Equations (24) and (25).

step 5: Update the position and pheromone size after the iteration.

step 6: If the end condition is satisfied, the optimal solution is obtained in the ant colony, or the maximum number of iterations has been reached. The iteration ends; otherwise, skip to step 3.

4.2. Improved Ant Colony Algorithm

In the classical ant colony algorithm, ants adjust the transition probability according to the pheromone concentration on the path and then choose the path [28]. The distribution of pheromone is very important for the ant's global path planning. At the same time, it needs a lot of time to filter the path in the initial stage of search, and the convergence speed is very slow. However, in the later stage of the ant colony algorithm, it needs to speed up the convergence rate and worry about falling into a local optimum. So, this article will improve the search method by adding a heuristic factor and pheromone concentration volatile coefficient.

In the previous section, the ant colony needs to conduct a global search according to the transition probability shown in Equation (24). When the transition probability is greater than the set transition probability, it needs to move to the best point. When it is less than the set transition probability, it will conduct a random search. This method undoubtedly wastes more time. At the same time, it causes the ant colony algorithm's early search range to be too large, and the convergence speed is slow. The higher the heuristic factor is, the closer the transition probability is to the greedy rule [29]. The transition probability Equation (24) can be changed to:

$$P_{i,best} = \frac{e^{\tau_{Xtbst)} - \tau_{X(i)}}}{e^{\tau_{X(b+t)}}} \eta_{i,best}. \tag{28}$$

The above formula shows that the probability of ant B in the current state transferring to the next point is not only affected by the pheromone concentration but also by the distance of the next point. The formula of $\eta_{i,best}$ can be obtained from Equation (29).

$$\eta_{i,best} = \frac{1}{d_{i,best}} = \frac{1}{\sqrt{(x_i - x_{best})^2 + (y_i - y_{best})^2}} \tag{29}$$

1. Global search

In the classical ant colony algorithm, the global search is carried out according to Equation (39). However, the random search ants in the global search are too loose, and the search time is too long. Therefore, in this paper, we will use the target attraction strategy to search the ants that are transferred to the best around the random search ants and select the next transfer direction of the ants according to the heuristic factor, as shown in Figure 6a. At this time ant i can not get close to the best. In order to avoid too long convergence time, the random search direction of ant i can be any ant within the radius. In order to be more efficient, we need to combine the heuristic factor to search and calculate the transition probability of ant i to n points within the radius. According to the direction of the largest transition probability, ant i moves to:

$$X_i = \begin{cases} X_i + \lambda(X_{best} - X_i), P_{i,best} > P_{set} \\ X_i + \lambda(X_j - X_i), P_{i,j} = max(P_{i,n}) \\ X_i + \text{rand}(-1,1) \cdot \frac{b-a}{M}, otherwise \end{cases} . \quad (30)$$

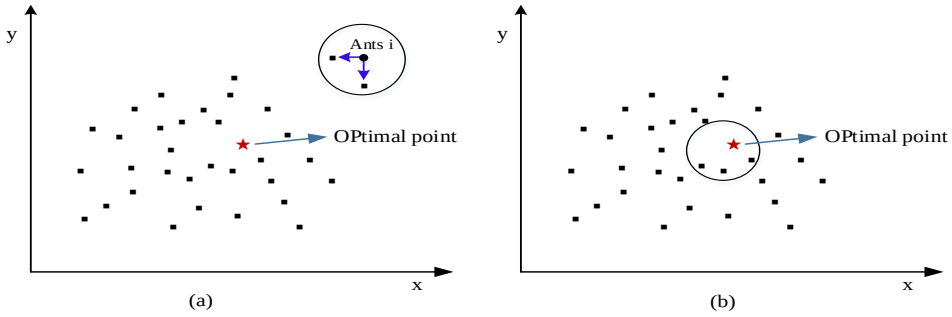

Figure 6. (**a**) Schematic diagram of random search path selection of ants. (**b**) Schematic diagram of ant local search path selection.

2. Local search

After the first iteration, the ant colony finds the optimal solution and then needs to carry out a local search in the next iteration, as shown in Figure 6b. In order to avoid falling into the local optimum prematurely, we should search in a large range as far as possible in the early stage of the search. With the increase of the number of iterations, the search radius should be gradually reduced. The search rules are as follows:

$$X_{is} = \begin{cases} X_{best} + \omega \cdot r, \text{rand}(-1,1) < 0.5 \\ X_{best} - \omega \cdot r, \ otherwise \end{cases} \quad (31)$$

where $\omega = 1 - 0.3 \cdot \frac{n}{n_{max}}$, and n and n_{max} represent the number of current iterations and the maximum number of iterations, respectively. At the same time, taboo list T_{abn} is added to global search and local search. According to the concept of taboo list, it refers to the position that the ant has already passed. Through the taboo list, the ant can be prevented from moving to the position that it has passed again, which wastes the search time.

4.3. Improvement of Volatile Factor

Volatility factor ρ is the coefficient of pheromone concentration volatility, which determines the search performance of ants and the feasibility of the algorithm. If the volatilization coefficient is set too small, the ant colony will have a strong guiding effect on the ants, leading to the lack of search ability of the ant colony system in the early stage. If the volatilization coefficient is set too large, the ant colony will have a weak guiding effect on the ants, and the convergence speed will be slow in the later stage. Some ants in the ant colony will repeatedly search the same location wasting resources. Based on the

above theory, an adaptive volatilization coefficient is proposed [30]. A larger volatilization coefficient is set in the early stage of the algorithm, so as to weaken the guiding role between ants and enhance the guiding performance. With the continuous decrease of volatilization coefficient, the volatilization coefficient will become very small in the later stage of the algorithm, so as to improve the convergence speed of ant colony search. The update rule of volatile coefficient is as follows:

$$\rho(t) = \begin{cases} 0.9\rho(t-1), \rho(t) \geqslant \rho_{min} \\ \rho_{min} \end{cases} \quad (32)$$

where ρ_{min} is the minimum volatile coefficient.

The flow of the improved ant colony algorithm is shown in Figure 7.

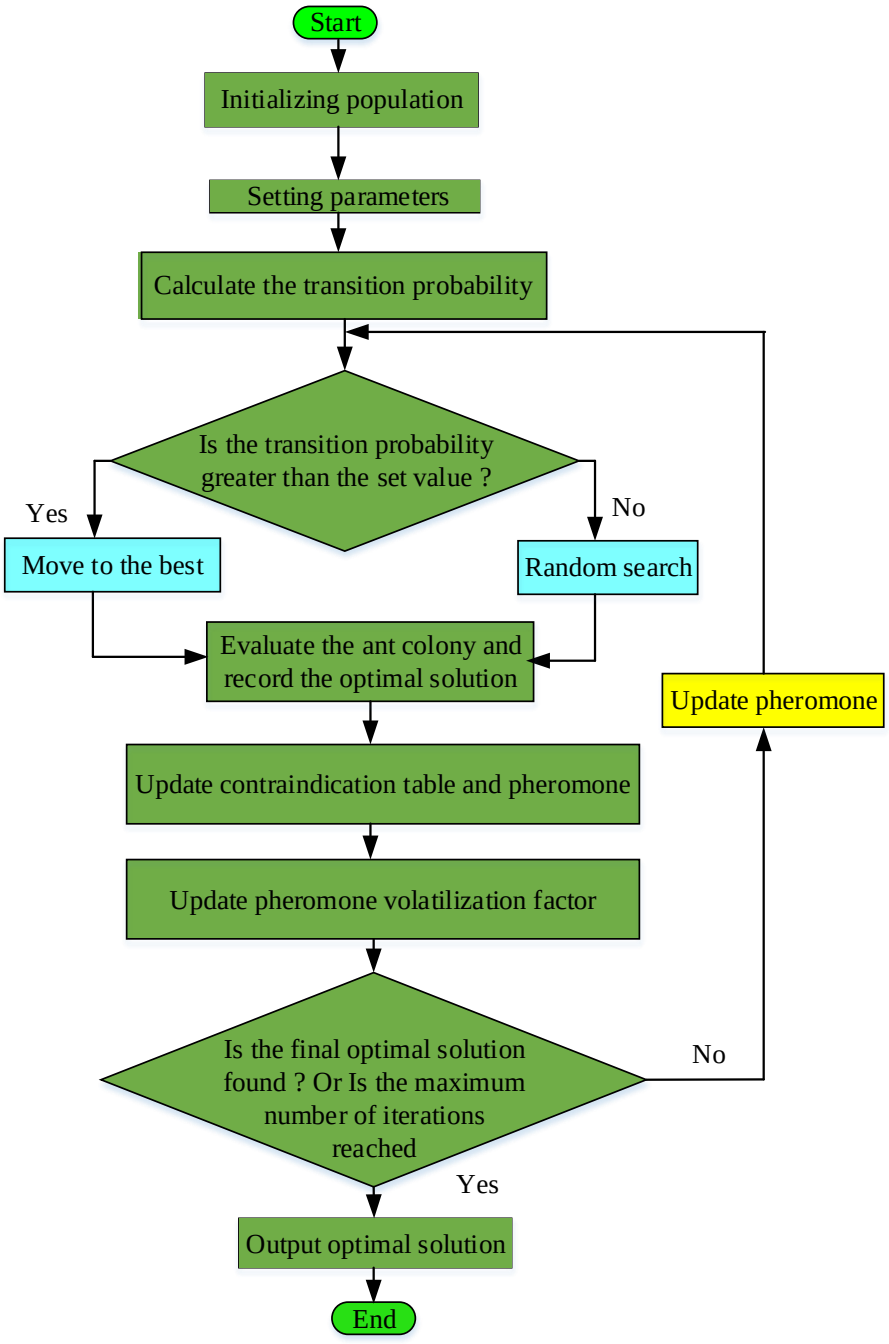

Figure 7. Improved flow chart of ant colony optimization (ACO).

4.4. Solve the Optimal Equivalent Factor

This section mainly uses the improved ant colony algorithm to optimize the equivalent factor of charging and discharging [24]. There are two objects to be optimized; the position of the ant is initialized as:

$$\begin{cases} x(i,1) = a(1) + \frac{b(1)-a(1)}{M}(i-1+\text{rand}(0,1)) \\ x(i,2) = a(2) + \frac{b(2)-a(2)}{M}(i-1+\text{rand}(0,1)) \end{cases} . \quad (33)$$

Among them, $x(i,1)$ and $x(i,2)$ represent the charge equivalent factor and discharge equivalent factor, respectively.

The independent variable is defined as the equivalent factor s, and the function value is the SOC deviation value at the end of the stroke—that is, the SOC final value minus the SOC hold value. When SOC deviation is 0, the optimal solution of the equation is obtained. The iteration process is shown in Figure 8. First, two initial equivalent factors are given; then, ECMS is used to simulate the whole ship model, and the deviation between ending SOC and target SOC is obtained. If the absolute value of the deviation meets the requirements, the iteration will be ended, and the optimal equivalent factor will be returned; if it does not meet the requirements, the next equivalent factor will be calculated, and then the ECMS algorithm will be called to simulate and calculate the SOC deviation. If the deviation is within the specified range, the optimal value will be returned; if it is not satisfied, the iteration will continue.

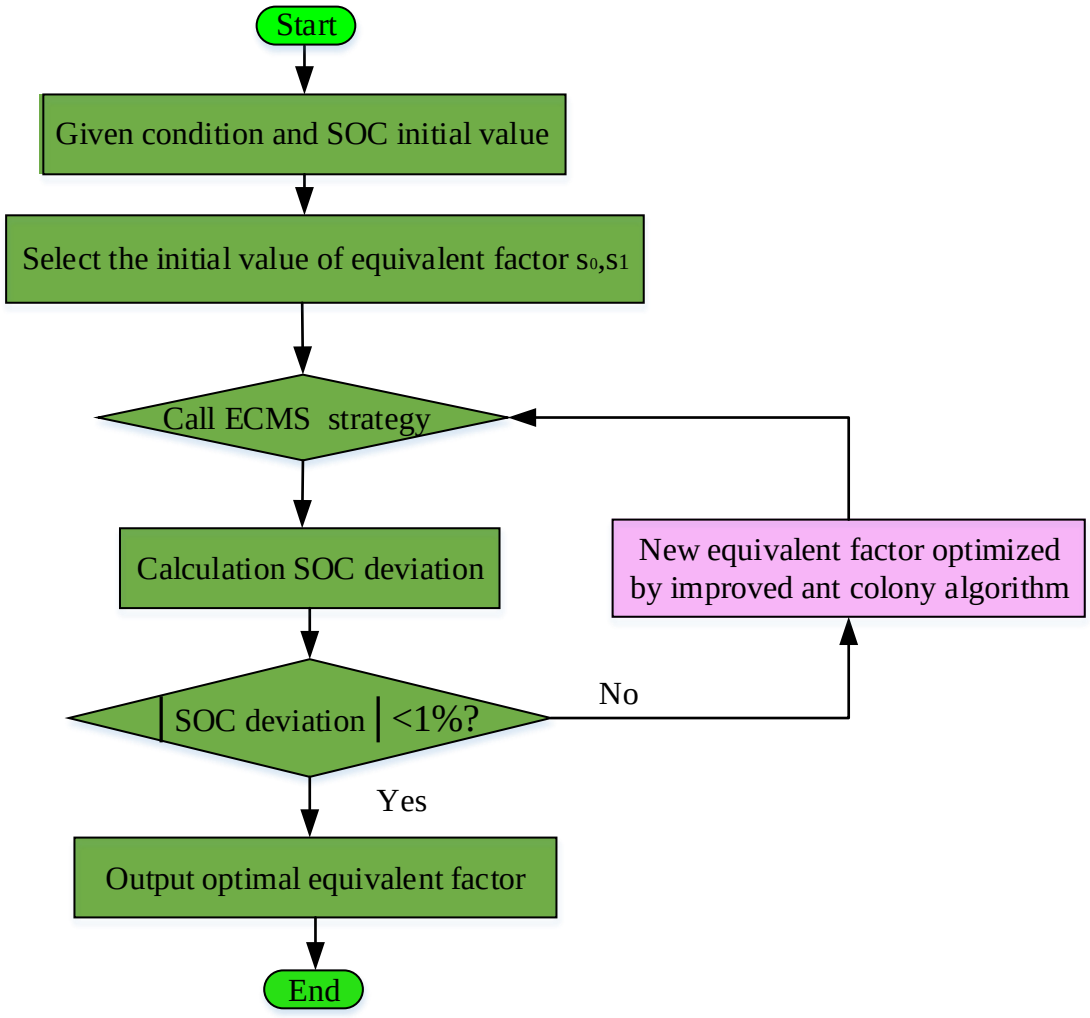

Figure 8. Optimal equivalent factor solution process.

5. Results

In order to verify the effect of ACO-ECMS energy management strategy in reducing fuel consumption and controlling SOC, a complete fishing operation condition (T) was used to simulate. The complete working condition (T) includes three parts: full speed section (T1), rope feeding section (T2), and rope lifting section (T3). A complete fishing operation condition (T) is shown in Figure 9a.

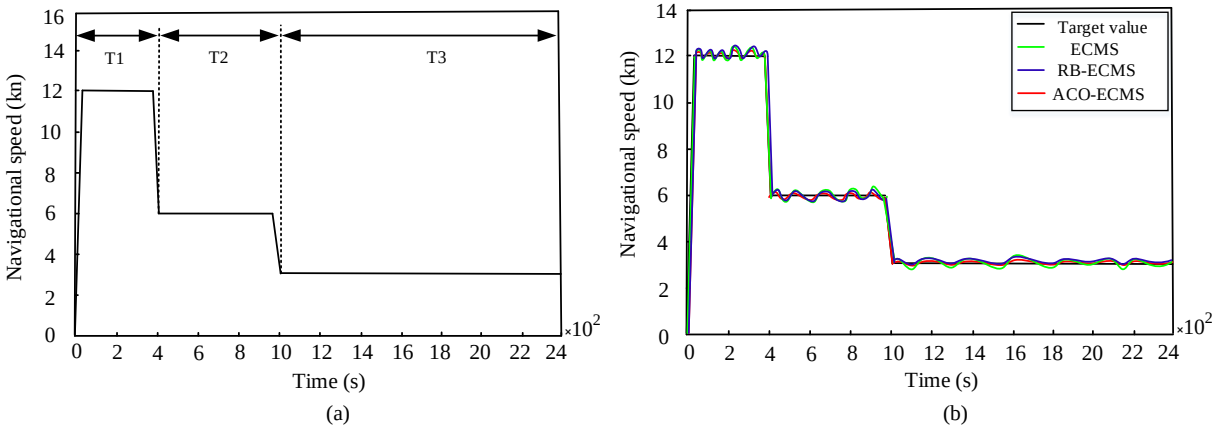

Figure 9. (**a**) A complete fishing operation condition (T). (**b**) Simulation results of speed under the T condition.

Figure 9b shows the speed simulation results of ACO-ECMS, RB-ECMS, and ECMS control strategy under the T condition. It can be seen that these three strategies can meet the speed demand, which can better track the target speed. Figure 10 shows the SOC simulation results of a complete operation condition. The initial value of SOC was 0.4. At the end of simulation, the SOC of the ACO-ECMS control strategy was 0.4008, the RB-ECMS control strategy was 0.409, and the ECMS control strategy was 0.412. It can be seen from Figure 10 that although both the ACO-ECMS and RB-ECMS control strategies can achieve SOC balance within the allowable deviation range, the effect of the ACO-ECMS control strategy is better than that of RB-ECMS control. The reason is that the implementation methods of the two strategies are different. ACO-ECMS is realized by iteratively optimizing the equivalent factor of the ACO algorithm; the RB-ECMS control strategy is realized by adjusting the working mode switching rules, which needs repeated debugging and verification by the engineers.

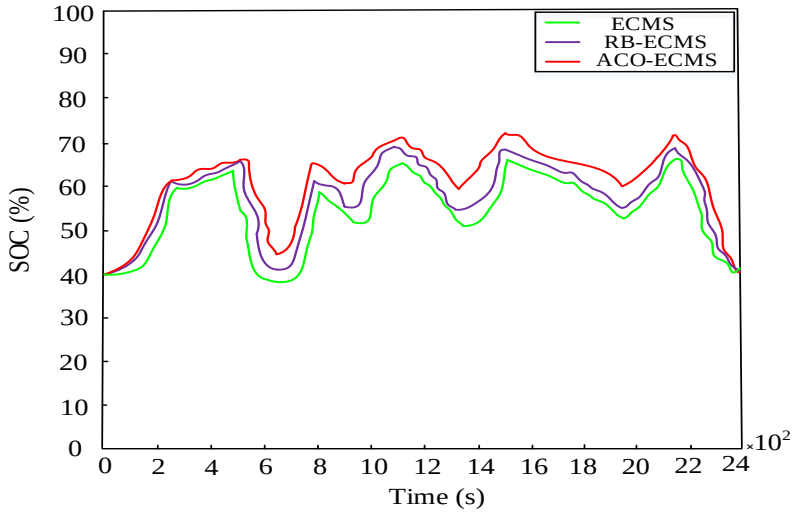

Figure 10. State-of-charge (SOC) simulation results of a complete operation condition.

Figures 11–13 show the power distribution curves of diesel engine and motor under the T condition with the ECMS strategy, RB-ECMS strategy, and ACO-ECMS strategy, respectively. The ECMS strategy charged the battery six times under the T condition. The RB-ECMS strategy and ACO-ECMS strategy were both utilized five times. Under the control of the ECMS strategy, the output power of the diesel engine and motor fluctuated slightly, and the operation of the diesel engine and motor was stable. The second was the RB-ECMS strategy. The output power fluctuation of the diesel engine and motor controlled by the ACO-ECMS strategy was smaller, and the operation of the diesel engine and motor was more stable. This shows that ACO has a good effect in optimizing the equivalent factor.

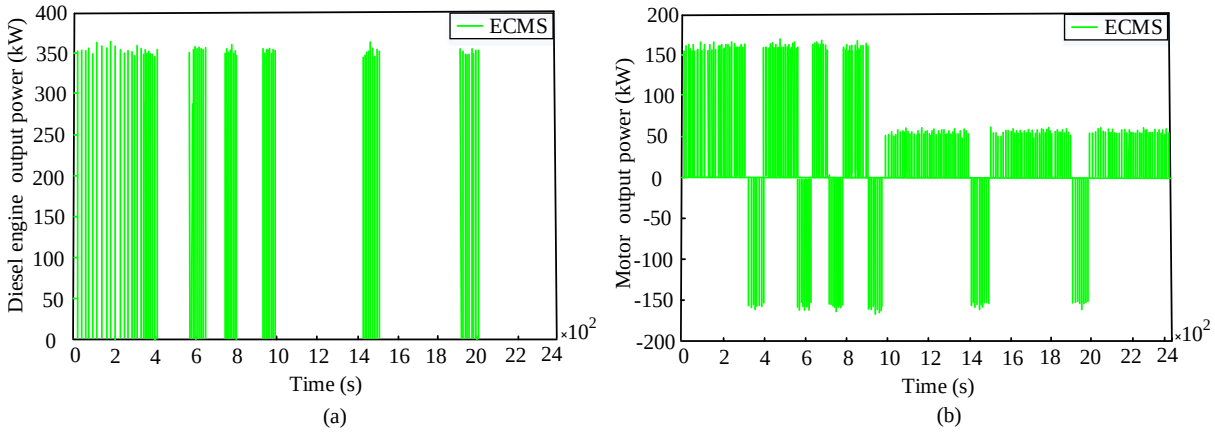

Figure 11. (**a**) Power distribution of ECMS strategy diesel engine under the T condition. (**b**) Power distribution of ECMS strategy motor under combined condition.

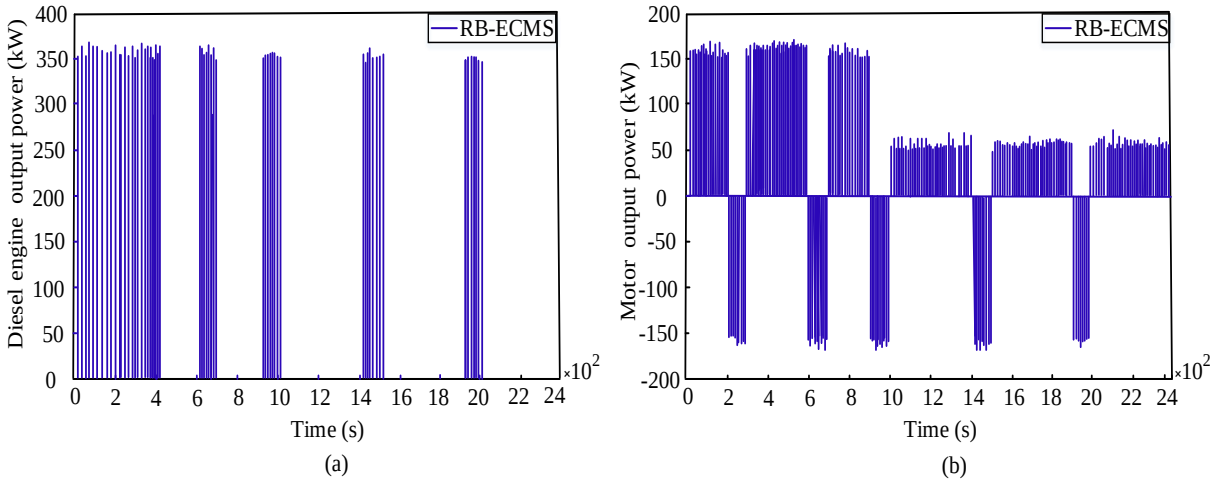

Figure 12. (**a**) Power distribution of rule-based (RB)-ECMS strategy diesel engine under the T condition. (**b**) Power distribution of RB-ECMS strategy motor under the T condition.

Figure 14 show the distribution and statistical results of engine operating points under the T condition. It can be seen from Figure 14a–c that the engine operating points of the ACO-ECMS control strategy are more distributed in the high efficiency area, followed by the RB-ECMS control strategy, and the engine operating points of the ECMS control strategy are relatively scattered. It can be seen from Figure 14d that when the specific fuel consumption was in the range of 205–210 g·(kW·h)$^{-1}$, the ACO-ECMS control strategy was 59.04%, the RB-ECMS control strategy was 50.86%, and the ECMS control strategy was 41.15%. When the specific fuel consumption is 210–215 g·(kW·h)$^{-1}$, the ACO-ECMS control strategy was 36.47%, the RB-ECMS control strategy was 31.1%, and the ECMS control strategy was 30.7%. It can be seen from Figure 14 that the specific fuel consumption

of the engine operating point in this region is lower, and the efficiency is higher in the ACO-ECMS control strategy. Meanwhile, the ECMS control strategy has higher specific fuel consumption and lower efficiency.

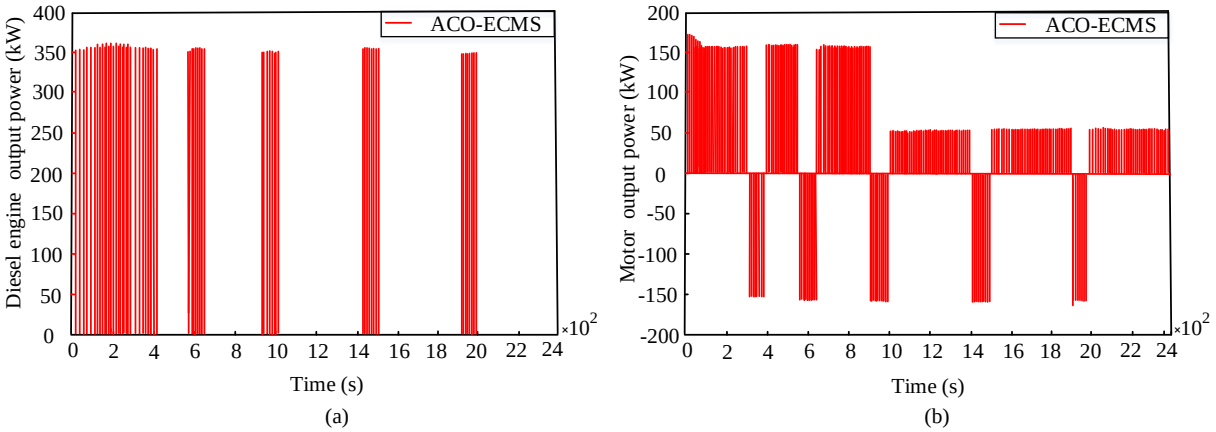

Figure 13. (**a**) Power distribution of the ant colony optimization (ACO)-ECMS strategy diesel engine under combined T conditions. (**b**) The motor power distribution of the PSO-DACO-ECMS strategy under T conditions.

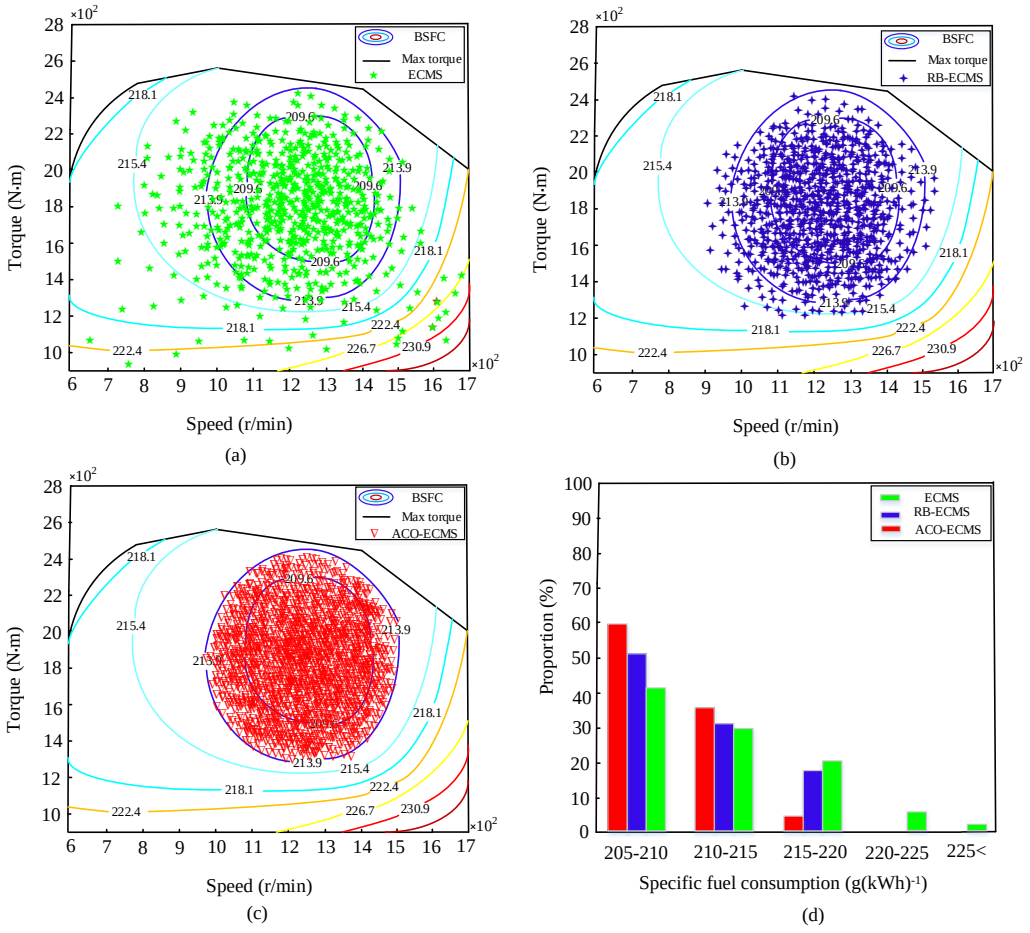

Figure 14. Comparison of fuel consumption rate of diesel engine with three control strategies (**a**) ECMS. (**b**) RB-ECMS. (**c**) ACO-ECMS. (**d**) Distribution statistics of engine operating points under the T condition.

Figure 15 shows the efficiency distribution diagram of motor working point under the T condition. It can be seen from Figure 15 that the motor of the ACO-ECMS control

strategy was in an efficient working area, followed by the RB-ECMS control strategy, and the distribution of motor operating points in the ECMS control strategy was relatively scattered. The simulation results show that the ACO-ECMS algorithm is superior to the RB-ECMS and ECMS algorithms in improving the efficiency of the diesel engine.

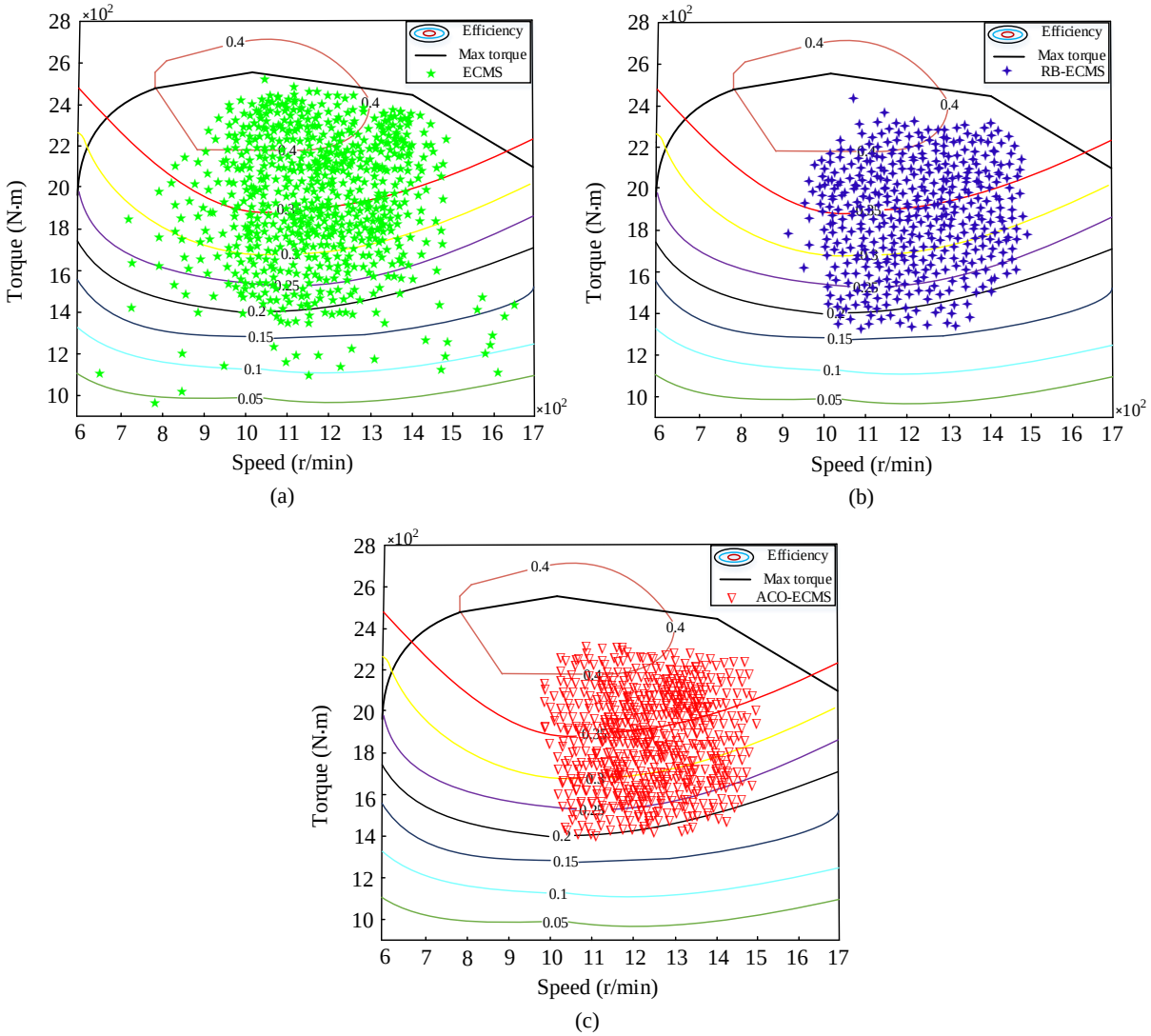

Figure 15. Comparison of three control strategies for diesel engine efficiency (**a**) ECMS. (**b**) RB-ECMS. (**c**) ACO-ECMS.

Figure 16 shows the working point distribution of three control strategies. It can be seen from Figure 16 that the motor of the ACO-ECMS control strategy was in an efficient working area, followed by the RB-ECMS control strategy, and the distribution of motor operating points in the ECMS control strategy is relatively scattered. This shows that the ACO algorithm is effective in optimizing the equivalent factor.

Taking a complete operation condition as an example, the fuel consumption of three control strategies is compared. Figure 17a shows the fuel consumption comparison of the three control strategies under the T1, T2, and T3 conditions.

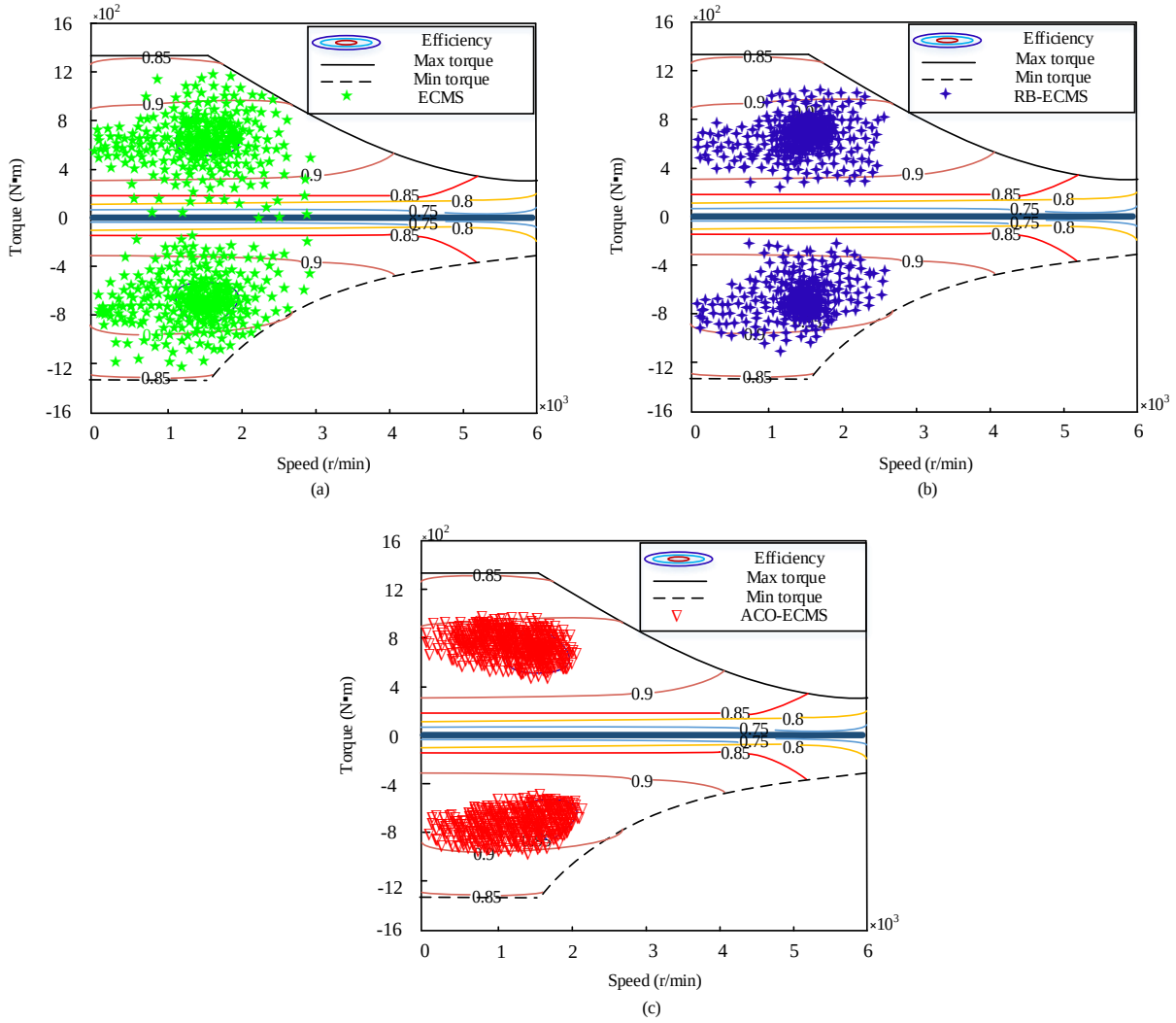

Figure 16. The comparison of motor operating points of three control strategies (**a**) ECMS. (**b**) RB-ECMS. (**c**) ACO-ECMS.

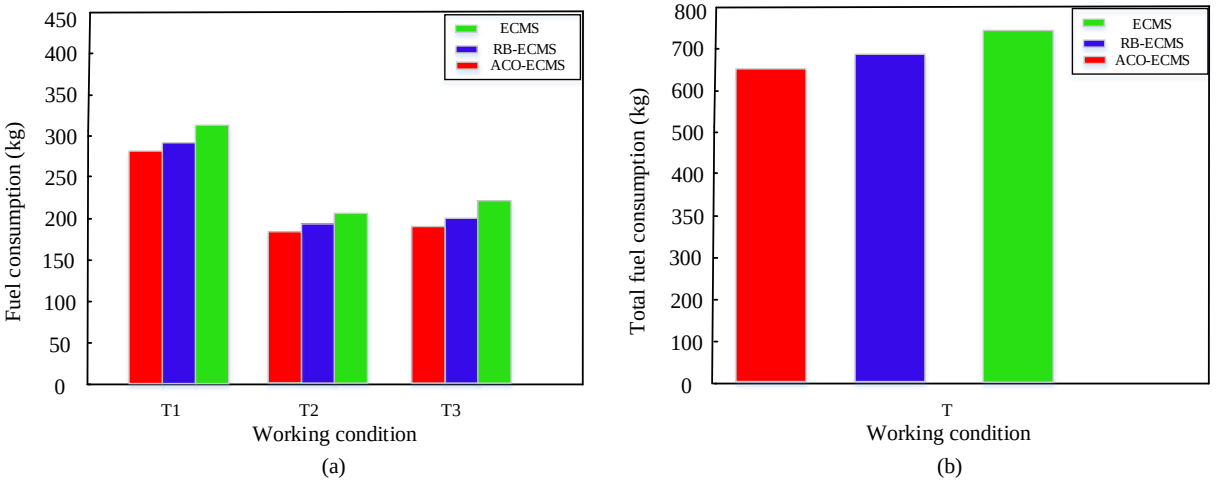

Figure 17. (**a**) The comparison of each condition fuel consumption. (**b**) The comparison of total fuel consumption.

In the T1 condition, the fuel consumption of ECMS, RB-ECMS, and ACO-ECMS were 278, 293, and 313 kg, respectively. In the T2 condition, the fuel consumption of ECMS, RB-ECMS, and ACO-ECMS were 183, 194, and 209 kg, respectively. In the T3 condition,

the fuel consumption of ECMS, RB-ECMS, and ACO-ECMS were 188, 201, and 217 kg, respectively. Figure 17b shows the total fuel consumption comparison. In the T condition, the total fuel consumption of ECMS, RB-ECMS, and ACO-ECMS were 649, 688, and 739 kg, respectively. Table 2 shows the statistics of fuel consumption under various working conditions. Compared with ECMS under the T condition, RB-ECMS and ACO-ECMS respectively reduced fuel consumption by 6.9% and 12.1%.

Table 2. Comparison of fuel economy for three methods.

Working Condition	Fuel Consumption (kg)		
	ECMS	RBB-ECMS	ACO-ECMS
T1	313	293	278
T2	209	194	183
T3	217	201	188
Total	739	688	649

6. Conclusions

In this paper, an energy management strategy combining an improved ACO algorithm with ECMS considering mode switching is proposed to save more fuel and control battery SOC. The simulation results showed that compared with the traditional ECMS control strategy, the RB-ECMS control strategy reduced fuel consumption by 6.9% and the ACO-ECMS control strategy reduced fuel consumption by 12.1% under the T condition. The difference between the final SOC value and the target value of the traditional ECMS control strategy was 0.012, the RB-ECMS control strategy was 0.009, and the ACO-ECMS control strategy was 0.0008. The proposed strategy can achieve the goal of ship fuel consumption reduction and control battery SOC. In addition, the effectiveness of the proposed strategy was verified on the simulation platform, which is crucial to the energy management system of parallel hybrid ships. Hence, the proposed strategy presents the significant potential for improved fuel economy controlled battery SOC for practical application. In the further study, an experimental scheme will be carried out on the bench of the parallel diesel electric hybrid ship test platform for verifying the performance of the ACO-ECMS control strategy.

Author Contributions: Conceptualization, Y.X.; methodology, Y.X.; software, X.Y.; validation, Y.X. and X.Y.; formal analysis, Y.X.; investigation, Y.X.; resources, X.Y.; data curation, Y.X.; writing—original draft preparation, Y.X.; writing—review and editing, Y.X.; visualization, Y.X.; supervision, Y.X.; funding acquisition, Y.X. All authors have read and agreed to the published version of the manuscript.

Funding: This research was funded by National Natural Science Foundation of China (NSFC) under Grant 51579200, and in part by Shenzhen Basic Research Project under Grant 20190805171545309.

Institutional Review Board Statement: Not applicable.

Informed Consent Statement: Informed consent was obtained from all subjects involved in the study.

Data Availability Statement: All data used to support the findings of this study are included within the article.

Conflicts of Interest: The authors declare no conflict of interest.

References

1. Kalikatzarakis, M.; Geertsma, R.D.; Boonen, E.J.; Visser, K.; Negenborn, R.R. Ship energy management for hybrid propulsion and power supply with shore charging. *Control Eng. Pract.* **2018**, *76*, 133–154. [CrossRef]
2. Gnes, P.; Pinamonti, P.; Reini, M. Bi-Level Optimization of the Energy Recovery System from Internal Combustion Engines of a Cruise Ship. *Appl. Sci.* **2020**, *10*, 6917. [CrossRef]
3. Skjong, E.; Johansen, T.A.; Molinas, M.; Sørensen, A.J. Approaches to economic energy management indiesel electric marine vessels. *IEEE Trans. Transp. Electrif.* **2017**, *3*, 22–35. [CrossRef]
4. Edrington, C.S.; Ozkan, G.; Papari, B. Distributed energy management for ship power systems with distributed energy storage. *J. Mar. Eng. Technol.* **2020**, *19*, 31–44. [CrossRef]

5. Yigit, K.; Acarkan, B. A new electrical energy management approach for ships using mixed energy sources to ensure sustainable port cities. *Sustain. Cities Soc.* **2018**, *40*, 126–135. [CrossRef]
6. Geertsma, R.D.; Negenborn, R.R.; Visser, K. Parallel control for hybrid propulsion of multifunction ships. *IFAC Pap.* **2017**, *50*, 2296–2303. [CrossRef]
7. Barelli, L.; Bidini, G.; Gallorini, F. Dynamic Modeling of a Hybrid Propulsion System for Tourist Boat. *Energies* **2018**, *11*, 2592. [CrossRef]
8. Frangopoulos, C.A. Developments, trends, and challenges in optimization of ship energy systems. *Appl. Sci.* **2020**, *10*, 4639. [CrossRef]
9. German-Galkin, S.; Tarnapowicz, D. Energy Optimization of the 'Shore to Ship System-A Universal Power System for Ships at Berth in a Port. *Sensors* **2020**, *20*, 3815. [CrossRef]
10. Gao, D.; Jiang, Y.; Zhao, N. A novel load prediction method for hybrid electric ship based on working condition classification. *Trans. Inst. Meas. Control* **2020**, 0142331220923767. [CrossRef]
11. Bassam, A.M.; Phillips, A.B.; Turnock, S.R. Development of a multi-scheme energy management strategy for a hybrid fuel cell driven passenger ship. International. *J. Hydrogen Energy* **2017**, *42*, 623–635. [CrossRef]
12. Tian, X.; Cai, Y.; Sun, X. An adaptive ECMS with driving style recognition for energy optimization of parallel hybrid electric buses. *Energy* **2019**, *189*, 116151. [CrossRef]
13. Tian, X.; He, R.; Sun, X.; Cai, Y.; Xu, Y. An ANFIS-Based ECMS for Energy Optimization of Parallel Hybrid Electric Bus. *IEEE Trans. Veh. Technol.* **2019**, *69*, 1473–1483. [CrossRef]
14. Bizon, N.; Thounthong, P. Fuel economy using the global optimization of the Fuel Cell Hybrid Power Systems. *Energy Convers. Manag.* **2018**, *173*, 665–678. [CrossRef]
15. Haseltalab, A.; Negenborn, R.R.; Lodewijks, G. Multi-level predictive control for energy management of hybrid ships in the presence of uncertainty and environmental disturbances. *IFAC Pap.* **2016**, *49*, 90–95. [CrossRef]
16. Dedes, E.K.; Hudson, D.A.; Turnock, S.R. Investigation of Diesel Hybrid systems for fuel oil reduction in slow speed ocean going ships. *Energy* **2016**, *114*, 444–456. [CrossRef]
17. Sun, C.; Sun, F.; He, H. Investigating adaptive-ECMS with velocity forecast ability for hybrid electric vehicles. *Appl. Energy* **2017**, *185*, 1644–1653. [CrossRef]
18. Gupta, V. ECMS based hybrid algorithm for energy management in parallel hybrid electric vehicles. *HCTL Open Int. J. Technol. Innov. Res.* **2015**, *14*, 2321-1814.
19. Sulaiman, N.; Hannan, M.A.; Mohamed, A.; Ker, P.J.; Majlan, E.H.; Dauda, W.R.W. Optimization of energy management system for fuel-cell hybrid electric vehicles: Issues and recommendations. *Appl. Energy* **2018**, *228*, 2061–2079. [CrossRef]
20. Zhu, J.; Chen, L.; Wang, X.; Yu, L. Bi-level optimal sizing and energy management of hybrid electric propulsion systems. *Appl. Energy* **2020**, *260*, 114134. [CrossRef]
21. Trovão, J.P.; Machado, F.; Pereirinha, P.G. Hybrid electric excursion ships power supply system based on a multiple energy storage system. *IET Electr. Syst. Transp.* **2016**, *6*, 190–201. [CrossRef]
22. Letafat, A.; Rafiei, M.; Sheikh, M.; Afshari-Igder, M.; Banaei, M.; Boudjadar, J.; Khooban, M.H. Simultaneous energy management and optimal components sizing of a zero-emission ferry boat. *J. Energy Storage* **2020**, *28*, 101215. [CrossRef]
23. Yang, R.; Yuan, Y.; Ying, R.; Shen, B.; Long, T. A novel energy management strategy for a ship's hybrid solar energy generation system using a particle swarm optimization algorithm. *Energies* **2020**, *13*, 1380. [CrossRef]
24. Wei, X. Task scheduling optimization strategy using improved ant colony optimization algorithm in cloud computing. *J. Ambient Intell. Humaniz. Comput.* **2020**, 1–12. [CrossRef]
25. Stodola, P. Hybrid ant colony optimization algorithm applied to the multi-depot vehicle routing problem. *Nat. Comput.* **2020**, *19*, 1–13. [CrossRef]
26. Ning, J.; Zhao, Q.; Sun, P.; Feng, Y. A multi-objective decomposition-based ant colony optimization algorithm with negative pheromone. *J. Exp. Theor. Artif. Intell.* **2020**, 1–19. [CrossRef]
27. Zhao, J.; Cheng, D.; Hao, C. An improved ant colony algorithm for solving the path planning problem of the omnidirectional mobile vehicle. *Math. Probl. Eng.* **2016**. [CrossRef]
28. Zhao, B.; Gui, H.; Li, H.; Xue, Y. Cold Chain Logistics Path Optimization via Improved Multi-Objective Ant Colony. *Algorithm IEEE Access* **2020**, *8*, 142977–142995. [CrossRef]
29. Wang, Y.; Chen, J.; Ning, W.; Yu, H.; Lin, S.; Wang, Z.; Pang, G.; Chen, C. A time-sensitive network scheduling algorithm based on improved ant colony optimization. *Alex. Eng. J.* **2020**, *60*, 107–114. [CrossRef]
30. Jiao, Z.; Ma, K.; Rong, Y.; Wang, P.; Zhang, H.; Wang, S. A path planning method using adaptive polymorphic ant colony algorithm for smart wheelchairs. *J. Comput. Sci.* **2018**, *25*, 50–57. [CrossRef]
31. Zhang, Z.; Ye, J.; Tan, D.; Feng, Z.; Luo, J.; Tan, Y.; Huang, Y. The effects of Fe_2O_3 based DOC and SCR catalyst on the combustion and emission characteristics of a diesel engine fueled with biodiesel. *Fuel* **2021**, *290*, 120039. [CrossRef]